The 8th Pacific Rim International Congress on Advanced Materials and Processing
Edited by: Fernand Marquis
TMS (The Minerals, Metals & Materials Society), 2013

Thermodynamic Analyses of Iron Oxides Redox Reactions

Wei Zhang, Juhua Zhang, Qiang Li, Yibo He, Biao Tang, Mingming Li, Zuoliang Zhang, Zongshu Zou*

(School of Materials & Metallurgy, Northeastern University, Shenyang 110004, China)
*Corresponding author: Zongshu Zou, zouzs@mail.neu.edu.cn

Key words: iron oxides; thermodynamic quantities; data fitting; redox reactions

Abstract: The thermochemical data of iron oxide redox reactions in various textbooks and handbooks are not consistent. To clarify such confusions, the elementary thermodynamic data of various iron oxides, carbon oxides, hydrogen and water vapor are used to calculate the changes of thermodynamic quantities such as enthalpy, entropy and Gibbs free energy of the redox reactions. The predominance area diagrams are then reconstructed according to the newly calculated Gibbs free energy changes. In order to fit the precise Gibbs free energy data, the constrained optimization method is adopted based on the mathematical modeling software Lingo 11. The reduction experiments are successfully carried out to verify the calculated eutectoid temperature. It is concluded with sixteen empirical thermodynamic equilibrium formulas and eight enthalpy values at 25°C for iron oxides reduced by CO and H_2, and the eutectoid temperature of the three iron oxide phases is 576°C.

1 Introduction

Gas-solid reduction reactions of the iron oxides exist not only in the non-blast furnace process but also in the shaft of blast furnace and even the reaction of some catalysis processes. Reduction of iron oxides by CO and H_2 are the main and the most important chemical reactions during these processes.

Thermodynamic data of the iron oxides reduction reactions, especially the enthalpy and Gibbs free energy are indispensable for design and operational optimization of ironmaking processes. However, it is found that the calculated thermodynamic equilibrium data of these reactions much differ from each other according to different references [1-7]. To undertake modern blast furnace mathematical modeling [8-10], more accurate thermodynamic data are required for the intrinsic and macro kinetic mathematical simulation of the related chemical reaction processes.

In this paper, the thermodynamic data from different textbooks, manuals and journal papers are reviewed and summarized. Then a mathematical model is established for calculation of the thermodynamic data of iron oxides reduction reactions based on elementary data of iron oxides from the most recognized thermochemical data base [11-13]. The program-computed thermodynamic equilibrium data are fitted by means of the generalized least squares method under some thermodynamic constraints. The agreement between data from the empirical formulas and different resources is discussed.

2 Overview of Thermodynamic Analyses in Literatures

Reviews of published studies on the gas-solid equilibriums in the iron-oxygen-carbon and iron-oxygen-hydrogen systems, and of the literature concerning the iron oxides reveal a surprising degree of confusion. The results from different investigators are not satisfactory in agreement and are often difficult of interpretation.

Referring to thermodynamic studies of the iron oxides reduction reactions, it can be dated back to the work by Braithwaite [14] in 1895. He showed that carbon monoxide is completely oxidized to dioxide by ferric oxide at 'low red heat'.

Baur and Glaessner [15] are the first to publish quantitative results in this field. They determined the equilibrium composition of gas in the related reactions of iron-carbon-oxygen system. And soon it was widely applied as the Baur-Glaessner diagram and predominance area diagram (Figure 1) in ferrous metallurgy, material science and catalysis technology [1-7]. Regardless of Boudouard reaction, the iron oxides reduction mechanisms are commonly described like this: $Fe_2O_3 \rightarrow Fe_3O_4 \rightarrow Fe$ below 570°C, $Fe_2O_3 \rightarrow Fe_3O_4 \rightarrow FeO \rightarrow Fe$ above 570°C. The eutectoid temperature of iron oxides in the Baur-Glaessner diagram is 570°C, but is experimentally and theoretically determined as 576°C recently [16].

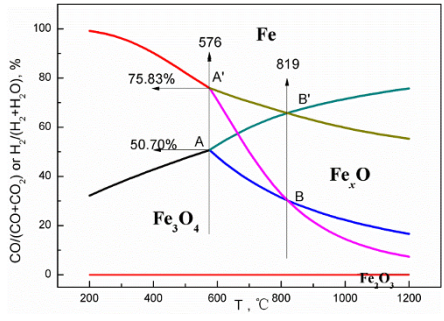

Figure 1 Predominance area diagram for iron oxides reduction reactions [16]

Schenck, Semiller and Falcke [17] have published data relating to the systems where, in addition to iron and ferrous oxide, solid carbon is present. Schenck & Heller [18] studied the system consisting of iron, ferrous oxide, and various forms of carbon. The work reported by Eastman and his partners [19-20] was undertaken in order to remove some of the more important uncertainties concerning the iron oxides reduction by CO and H_2. The sources of error in the measurements were investigated, the results were compared with those from other observers, and best values tabulated at round temperatures. Emmett and Shultz [21-22] obtained experimental results for the equilibrium constants of the FeO–Fe, Fe_3O_4–FeO, and Fe_3O_4–Fe systems by using a dynamic rather than a static apparatus. On account of the importance of ferrous oxide in many metallurgical reactions, the equilibria of iron and its oxides with steam and hydrogen has been investigated in the range 1200-1515°C by Chipman and Marshall [23].

After 1945, Darken and Gurry [24-25] established the iron-oxygen phase diagram and illustrated that the stoichiometric FeO could not stably exist under the ordinary pressure. In the iron-oxygen

system, FeO will readily dissociate into the more stable configuration composed of Fe and Fe_xO, where x is smaller than unity. The wustite phase, which has the same crystal structure as NaCl, remains deficient in iron even saturated with iron. The oxygen sites in the lattice are fully occupied, but some iron sites remain vacant.

3 Fitting of the Newly Calculated Thermodynamic Data

The newly calculated data for the equilibria of iron oxides reduction reactions are based on the most recognized thermodynamic data [11-13] and verified by experimental results [16]. For the sake of convenient utilization of the data, all the calculation results of the equilibrium constants are fitted in forms of concise empirical formulas in the following.

For achieving empirical formulas of the iron oxides reduction reactions, an application program is developed and used to calculate the accurate thermodynamic equilibrium data, and the generalized least squares method is used to fit the calculated data. Especially, the fitting is also restricted by the thermodynamic restraint conditions. Finally, the dependences of the equilibrium constants on temperature are obtained.

3.1 Thermodynamic Calculation Model [16]

For the reduction of iron oxides by CO, five chemical reactions are considered as follows

$$3Fe_2O_3 + CO = 2Fe_3O_4 + CO_2 \tag{1}$$

$$\frac{x}{4x-3}Fe_3O_4 + CO = \frac{3}{4x-3}Fe_xO + CO_2 \tag{2}$$

$$Fe_xO + CO = xFe + CO_2 \tag{3}$$

$$\frac{1}{4}Fe_3O_4 + CO = \frac{3}{4}Fe + CO_2 \tag{4}$$

$$Fe_xO = \frac{1}{4}Fe_3O_4 + \frac{4x-3}{4}Fe \tag{5}$$

Among these five equations, only three ones are free, and Eq. (5) is solid-solid reaction while the others are gas-solid reactions. For Eqs. (1)-(4),

$$\frac{100 - CO\%}{CO\%} = K^{\theta} = \exp(-\frac{\Delta G^{\theta}(T)}{RT}) \tag{6}$$

For pure substances, the relationship between Cp and T is,

$$C_p(T) = A_1 + A_2T + A_3T^{-2} + A_4T^2 + A_5T^{-3} \tag{7}$$

Since the Gibbs free energies of substances are a state functions related to temperature, the absolute value of G cannot be given. However, the relative Enthalpy, Entropy and Gibbs free energy of a substance i at temperature T can be defined as follows according to the *Kirchhoff's Formula*,

$$H_{T,i}^{\Theta} = H_{298}^{\Theta} + \int_{298}^{T} C_{p,i}(T)\,\mathrm{d}T + L_1 + \int_{T_1}^{T_2} C_{p,i}(T)\mathrm{d}T + L_2 + \ldots\ldots \quad (8)$$

$$S_{T,i}^{\Theta} = S_{298}^{\Theta} + \int_{298}^{T} \frac{C_{p,i}(T)}{T}\mathrm{d}T + \frac{L_1}{T} + \int_{T_1}^{T_2} \frac{C_{p,i}(T)}{T}\mathrm{d}T + \frac{L_2}{T} + \cdots \quad (9)$$

$$G_{T,i}^{\Theta} = H_{T,i}^{\Theta} - TS_{T,i}^{\Theta} \quad (10)$$

where L_1, L_2, … are phase transition enthalpies at the corresponding temperature T_1, T_2, …. Then the Gibbs free energy change of a chemical reaction can be calculated with Eq. (11).

$$\Delta G^{\Theta}(T) = \sum_i \nu_i G_{T,i}^{\Theta} = \sum_i \nu_i H_{T,i}^{\Theta} - T\sum_i \nu_i S_{T,i}^{\Theta} \quad (11)$$

As the stoichiometric substance FeO is instable, it is substituted by $Fe_{0.947}O$ in this calculation model.

3.2 Forms of the Fitting Formulas

According to Eq. (7), *Gibbs-Helmholtz* equation (12) and *Kirchhoff* equation (13), Eq. (14) and Eq. (15), it can be obtained.

$$\mathrm{d}\left(\frac{\Delta G_T^{\Theta}}{T}\right) = -\frac{\Delta H_T^{\Theta}}{T^2}\mathrm{d}T \quad (12)$$

$$\mathrm{d}\Delta H_T^{\Theta} = \Delta C_P \mathrm{d}T \quad (13)$$

$$\Delta H_T^{\Theta} = \Delta A_1 T + \frac{1}{2}\Delta A_2 \times T^2 - \Delta A_3 \times T^{-1} + \frac{1}{3}\Delta A_4 \times T^3 - \frac{1}{2}\Delta A_5 \times T^{-2} + A_6 \quad (14)$$

$$\Delta G_T^{\Theta} = -\Delta A_1 T \ln T - \frac{1}{2}\Delta A_2 T^2 - \frac{1}{2}\Delta A_3 T^{-1} - \frac{1}{6}\Delta A_4 T^3 - \frac{1}{6}\Delta A_5 T^{-2} + A_6' T + A_6 \quad (15)$$

where A_6 and A_6' are integration constants, and can be calculated according to Eq. (11) at 298K.

In a narrow temperature range, enthalpy change of a reaction can be regarded as constant as value of A_6 in Eq. (14), and the corresponding Gibbs free energy change can be expressed as $a + bT$, where a equals the value of enthalpy change. Actually, the first part of the Gibbs free energy change formula of a reaction a, is not equal to the enthalpy change in a considerable temperature range.

So $\Delta G^{\Theta} = a + bT$ is taken as the common fitting of Gibbs free energy change formula of a reaction, and $\Delta G^{\Theta} = a + bT + cT^2$ for a more precise approach. At the same time, enthalpy change of a reaction at 298K is also given for heat balance calculation.

3.3 Constraint Conditions [16]

The computer calculated thermodynamic equilibrium curves of these reactions differ remarkably from each other according to various references. To settle this confusion, the most

important object of this work is to attain the standard and authoritative dependence of the thermodynamic equilibrium data on temperature. In view of this, the precise computed results are used for fitting and two thermodynamic principles are set up as mathematical constraint conditions.

3.3.1 Three-curve-intersection Principle

The 'three-curve-intersection principle' means when iron oxides are reduced by CO or H_2, three balanced reduction potential curves of $Fe_xO \rightarrow Fe$, $Fe_3O_4 \rightarrow Fe$ and $Fe_3O_4 \rightarrow Fe_xO$, should absolutely meet at a certain point.

Taking the reduction by CO as an example, when the temperature is given, the value of ΔG^{Θ} and the corresponding reduction potential CO% of a reaction should be both unique according to Eq. (6). For the Gibbs free energy is a monotonous function of temperature, there must be a temperature point T_0 satisfying $\Delta G^{\Theta}{}_5(T_0) = 0$.

And additionally,

$$\Delta G^{\Theta}{}_2 = \Delta G^{\Theta}{}_3 - \frac{4x}{4x-3} \times \Delta G^{\Theta}{}_5 \tag{16}$$

$$\Delta G^{\Theta}{}_2 = \Delta G^{\Theta}{}_4 - \frac{3}{4x-3} \times \Delta G^{\Theta}{}_5 \tag{16'}$$

Consequently,

$$\Delta G^{\Theta}{}_2 \Big|_{T=T_0} = \Delta G^{\Theta}{}_3 \Big|_{T=T_0} = \Delta G^{\Theta}{}_4 \Big|_{T=T_0} \tag{17}$$

$$\mathrm{CO\%}_2 \Big|_{T=T_0} = \mathrm{CO\%}_3 \Big|_{T=T_0} = \mathrm{CO\%}_4 \Big|_{T=T_0} \tag{18}$$

So one can say that the three balanced reduction potential curves of $Fe_xO \rightarrow Fe$, $Fe_3O_4 \rightarrow Fe$ and $Fe_3O_4 \rightarrow Fe_xO$ intersect together at the temperature point T_0 (A in Figure1). Similar method can be used to prove that the diagram of iron oxides reduction by H_2 also obeys this principle (see point A' in Figure1).

3.3.2 Three-line-parallel Principle

As shown in Figure1, the reduction curves of Fe_3O_4, Fe_xO with CO and H_2 intersect at B and B' respectively. Three lines in this principle are lines AA', BB' and the vertical axis line respectively.

According to the three-curve-intersection principle, A' must have the same temperature value as A and equals T_0. As a result, line AA' and the vertical axis parallel each other.

To demonstrate the liaison between lines AA' and BB', reductions of iron oxides by H_2 should be considered.

$$3Fe_2O_3 + H_2 = 2Fe_3O_4 + H_2O \tag{1'}$$

$$\frac{x}{4x-3}Fe_3O_4 + H_2 = \frac{3}{4x-3}Fe_xO + H_2O \tag{2'}$$

$$Fe_xO + H_2 = xFe + H_2O \tag{3'}$$

$$\frac{1}{4}Fe_3O_4 + H_2 = \frac{3}{4}Fe + H_2O \tag{4'}$$

Point B is the intersection of reduction potential curves of Eqs. (2) and (2'), and point B' represents that of Eqs. (3) and (3'). Take point B for instance,

$$\frac{100 - CO\%}{CO\%} = K_2^{\ominus}|_{T=T_B}\ ; \quad \frac{100 - H_2\%}{H_2\%} = K_{2'}^{\ominus}|_{T=T_B} \tag{19}$$

The value of CO% and H_2% are equal to each other at point B, thus

$$K_2^{\ominus}|_{T=T_B} = K_{2'}^{\ominus}|_{T=T_B} \tag{20}$$

Furthermore, on the basis of *Hess' law*, subtracting Eq. (2') from Eq. (2), one obtains,

$$CO + H_2O = CO_2 + H_2 \tag{21}$$

Combination of Eqs. (19)-(21) leads to,

$$K_{21}^{\ominus}|_{T=T_B} = \frac{K_2^{\ominus}|_{T=T_B}}{K_{2'}^{\ominus}|_{T=T_B}} = 1\ ; \quad -\frac{\Delta G_{21}^{\ominus}(T)}{RT} = \ln\left(K_{21}^{\ominus}|_{T=T_B}\right) = 0 \tag{22}$$

The left part of Eq. (22) is a monotonous function of temperature, hence there must be a unique temperature point T_0', which equals accurately to T_B to satisfy the identical relation of Eq. (22). In the same way, it can be deduced as well that T_B' is also equal to T_0'. Therefore, lines BB', AA' and the vertical axis parallel naturally each other, and that's what the three-line-parallel principle tells.

As illustrated on Figure1, the whole plot is divided into four predominant phase areas by the equilibrium reduction potential curves of reactions (1)-(4) or (1')-(4'). Below the eutectoid temperature point 576℃, hematite can be reduced into magnetite and then iron in order; and when above 576℃, magnetite will undergo the wustite phase before being reduced into iron. As a result, perfect thermodynamic consistency principle was revealed during the logical deduction of the three-curve-intersection rule and three-line-parallel rule. However, the two rules could not be satisfied with the empirical equilibrium data from most textbooks [1-7].

3.4 Mathematical Model and Fitting Results

According to the thermodynamic principle, to satisfy the 'three-curve-intersection' means to satisfy the equilibrium of reaction (5); to satisfy the 'three-line-parallel principle' implies to make the reaction (21) reach balance. Therefore, the mathematical model for the fitting process is determined as Eqs. (23)-(25).

$$\min = \sum_{j=1}^{N}\left[G_{i,j} - \left(A + BT_{i,j} + CT_{i,j}^2\right)\right]^2 \tag{23}$$

$$G^{\ominus}_{R(i),\ 849} = H^{\ominus}_{849,\ i} - 849 \times S^{\ominus}_{849,\ i} \tag{24}$$

$$G^{\ominus}_{R(21),\ 1092} = G^{\ominus}_{R(2),\ 1092} - G^{\ominus}_{R(2'),\ 1092} = G^{\ominus}_{R(3),\ 1092} - G^{\ominus}_{R(3'),\ 1092} = 0 \tag{25}$$

where $G_{i,j}$ denotes precise Gibbs free energy change of reaction i (i=1-4, 1'-4') for a certain temperature with a group number j=1, 2,...N. $T_{i,j}$ denotes the corresponding temperature, and $G^{\Theta}_{R(i),T}$ represents approximate Gibbs free energy change of a reaction i at a temperature value of T after fitting. When $\Delta G^{\Theta} = a + bT$ is used as the fitting formula, constant C in Eq. (23) equals 0.

According to the thermodynamic calculation model, equilibrium equations of reactions (1)-(4) and (1')-(4') (x=0.947) can be calculated on the basis of Eqs. (6)-(11). Moreover, the characteristic data were drawn in Figure1 and the results agree fairly with the three-curve-intersection principle and the three-line-parallel principle.

For attaining empirical formulas of the iron oxides reduction reactions, an application program is used to compute the accurate thermodynamic equilibrium data, and the generalized least squares method is used to fit the calculated data. Especially, the fitting has been restricted by the thermodynamic restraint condition as Eqs. (24)-(25). Finally, the dependences of Gibbs free energies with concise forms and equilibrium constants on temperature are obtained and listed in Table I. It can be concluded that the standard deviations with restraints are greater than those without constraint conditions. After all, all the standard deviations are small enough and the linear correlation coefficients are good enough. To examine the fitting extent, an approximate Baur-Glaessner plot is given under a background of the precisely calculated data in Figure 2(*a*).

Table I. Fitting results for reactions (1)-(4) and (1')-(4')

Reaction-range/°C	$\Delta G^{\Theta} = a + bT$, J·mol^{-1}		$K^{\Theta}=\exp(c + d/T)$		Standard Deviation		Correlation Coefficient
	a	*b*	*c*	*d*	$S^*\|_{free}$	$S^*\|_{restraint}$	
R(1)-(25~1462)	-42639	-47.39	5.700	5128.6	0.083	-	-0.9997/58
R(2)-(576~1377)	26044	-30.44	3.661	-3132.5	1.02E-04	0.32	-
R(3)-(576~1377)	-18628	22.17	-2.667	2240.6	1.27E-04	1.33E-03	0.9998/33
R(4)-(300~576)	-8287	9.993	-1.202	996.75	3.1E-05	1.1E-04	0.9964/12
R(1')-(300~1462)	-11917	-75.52	9.083	1433.37	-	-	-
R(2')-(576~1377)	61473	-62.88	7.563	-7393.9	3.14E-04	3.67E-03	1.0000/33
R(3')-(576~1377)	16826	-10.30	1.239	-2023.8	3.94E-04	0.36	-
R(4')-(300~576)	29369	-25.07	3.015	-3532.5	2.4E-04	8.3E-04	-0.9987/12

$S^*|_{free}$: Standard deviation with no restraint;

$S^*|_{restraint}$: Standard deviation with restraint of 'three-curve-intersection' or 'three-line-parallel' or both.

In order to attain more precise equations, polynomial fitting with thermodynamic restraint conditions is undertaken on the basis of Eq. (23)-(25). The fitting results are listed in Table II and plotted in Figure 2(b). It is clear that the quadratic polynomial fitting is better than linear fitting. Meanwhile, the enthalpies for reactions (1)-(4) and (1')-(4') at 298K are also given in Table II. In addition, the linear formulas of the Gibbs free energy changes are accurate enough to meet requirement for most cases. So the linear expressions are highly recommended for simple

process calculations and the quadratic polynomial equations are suggested in computer programming processes.

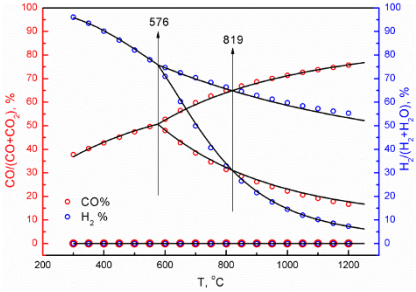

(*a*) Linear regression results

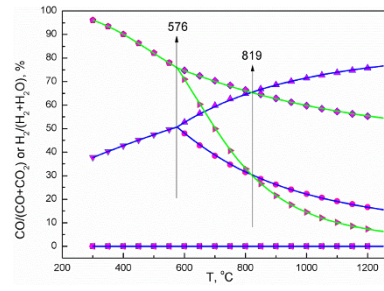

(*b*) Quadratic polynomial fitting results

Figure 2 Fitted plot of equilibrium data of the iron oxides reduction reactions

Table II. Quadratic polynomial regression results for Gibbs free energy changes

Reaction-range/°C	$\Delta G^{\theta} = a + bT + cT^2$, **J·mol^{-1}**			ΔH^{θ} **(298K),**
	a	***b***	***c***	**kJ·mol^{-1}**
R(1)-(25~1462)	-41223.1	-50.811	1.687×10^{-3}	-43.22
R(2)-(576~1377)	26195.9	-29.814	-9.437×10^{-4}	47.36
R(3)-(576~1377)	-21339.5	27.225	-2.190×10^{-3}	-16.69
R(4)-(300~576)	-2641.0	-5.588	1.052×10^{-2}	-3.37
R(1')-(300~1462)	-667.676	-93.338	6.622×10^{-3}	-2.07
R(2')-(576~1377)	65584.7	-70.528	3.309×10^{-3}	88.51
R(3')-(576~1377)	18049.1	-13.488	2.062×10^{-3}	24.46
R(4')-(300~576)	39118.8	-52.017	1.821×10^{-2}	37.78

4 Discussion

The most important object of this work is to determine the ideal thermodynamic data of the iron-carbon-oxygen and iron-hydrogen-oxygen systems for ironmaking designs and calculations. As the fitted data are shown above, the fitness of the regression formulas will be discussed in the following four aspects.

4.1 Agreement with Constraint Conditions

Taking advantage of these approximate formulas, the final Baur-Glaessner diagram is drawn in Figure 2 and it strictly obeys the three-curve-intersection principle and three-line-parallel principle, while data from the cited textbooks [1-7] and journals [30-31] cannot meet these rules. Comparisons of the calculation results with different thermodynamic equilibrium formulas from different references are plotted in Figure 3 where the doted curves are the accurate calculation results.

The constraint satisfaction of results from various studies is examined with the

computer-calculated results as base case. The results, including the deviation error, are listed in Table III. As the table shown, it is concluded that, except for the results from HSC Chemistry and the present work, all the others cannot simultaneously meet the two rules mentioned above.

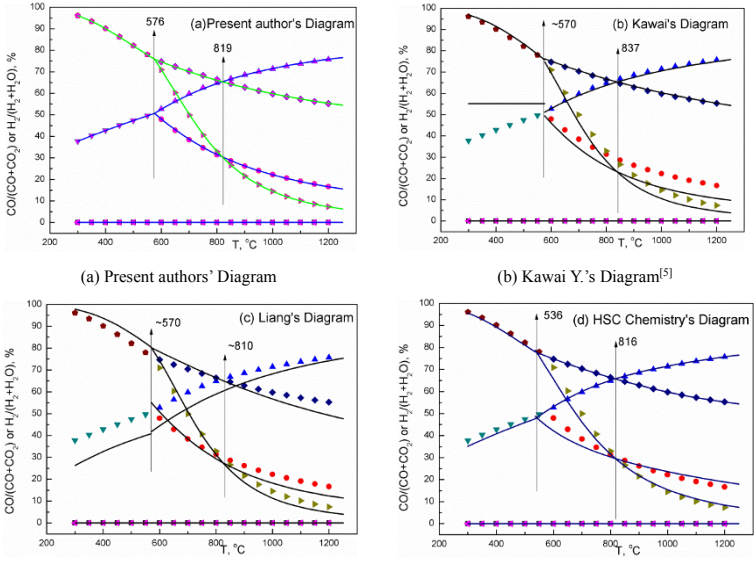

(a) Present authors' Diagram (b) Kawai Y.'s Diagram[5]

(c) Liang L. K.'s Diagram[2] (d) HSC Chemistry 6's Diagram

Figure 3 Comparisons of calculation results according to different data from different references [16]

Table III. Comparison of constraint satisfaction of results from various studies

No.	Reference	Authors	Intersection principle		Parallel principle	
			Yes / No	Error/%	Yes / No	Error/%
0	[13]	BARIN I.	Yes	0	Yes	0
1	[2]	LIANG L. K.	No	-3.8~12.8	No	0.73~6.8
2	[3]	KIRKALDY J. S.	Yes	-1.7	No	0.85~3.8
3	[4]	RAO Y. K.	Yes	1.4	Unknown*	7.9
4	[5]	KAWAI Y.	No	-6.8~10.2	No	3.8
5	[6]	JOHN F. E.	Yes	-2.8	Unknown*	0.73
6	-	HSC Chemistry	Yes	-6.9	Yes	-1.1
7	-	Present work	Yes	0.0	Yes	0.0

* Lack of H_2 reduction data or not explicit results.

4.2 Agreement with Standard Data

As we all know, Barin's data [11, 13] have a good agreement with that of NIST's [12], so here the

fitness of some representative data [4, 5] is just examined with standard results from the established thermodynamic calculation program.

Figure 3 shows the comparisons of different thermodynamic calculation results of iron oxide reduction reactions from various sources. It is clear that data from the present work and HSC Chemistry are much better than that from other sources on agreement with the standard one (dotted curves).

The errors of the balanced reduction potential of Fe_2O_3-Fe_3O_4 from all references are nearly 0.0%, so they are not presented and compared.

4.3 Eutectoid Temperature

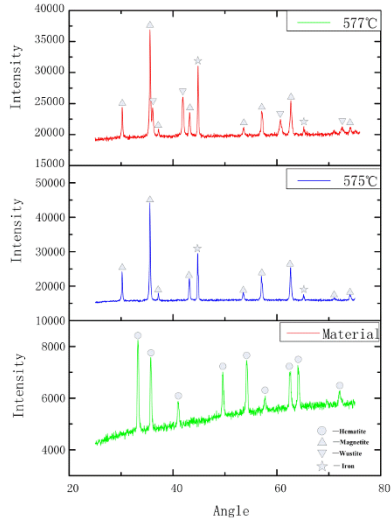

Figure 4 X-ray diffraction patterns of the starting material and final products after reduction [16]

Eutectoid temperature of the three iron oxide phases in CO-CO_2 or H_2-H_2O atmosphere differs from each other in the references [1-7, 15-29], usually in the range of 560~580℃. It's 536℃ according to the HSC Chemistry, which is -4.5% deviated from the computer-calculated data in the present work. To determine the real eutectoid temperature, a hematite reduction experiment is conducted and the reduction products are analyzed.

Hematite powders with a purity of 99.0% are used as the starting material. The equipment is a differential thermal analyzer STA 409CD. In the experiment, the furnace atmosphere is first cleansed from air by pure CO and then the material is heated to a pointed temperature in the atmosphere with a heating rate of 40K/min. After reduction by pure CO for 20 minutes, the material was cooled to room temperature under CO atmosphere. Finally, the crystal phases of the reduction products are examined with X-ray diffraction.

As displayed in Figure 4, the final products are magnetite and iron when the powders are

reduced by CO for 20 minutes at 575℃. After reduction at 577℃, there are magnetite, wustite and iron in the final product. Besides, iron carbide is not observed in both cases, and this agrees with literatures report [32-35]. The absence of carbide may be attributed to the sharp temperature rising, and it is hard to detect a tiny quantity of carbide. To conclude, the eutectoid temperature of the three phases of Fe_xO, Fe and Fe_3O_4, is limited in the range of 575~577℃.

4.4 Enthalpy Changes of Reactions

Table IV. Comparisons of enthalpy between different authors

Resources	ΔH^{θ} (298K), kJ·mol^{-1}							
	R(1)	R(2)	R(3)	R(4)	R(1')	R(2')	R(3')	R(4')
Present work	-43.22	47.36	-16.69	-3.37	-2.07	88.51	24.46	37.78
Kawai [5]	-27.61	35.11	-17.50	0	5.69	68.50	15.82	33.35
Zhu [28]	-53.60	40.60	-18.83	-3.97*	-12.10	82.00	22.60	37.45*
Wang [26]	-67.24	22.40	-13.19	-25.29	-21.81	63.60	28.01	20.52
HSC	-44.96	44.06	-16.66	-4.09	-3.83	85.20	24.47	37.05

* Data of R(4) and R(4') from Zhu's textbook are calculated according to *Hess' law*.

Enthalpy data from different resources are gathered and compared in Table IV. It should be noted differences of stoichiometric numbers between FeO and $Fe_{0.947}O$ are neglected in ordinary textbooks. So according to *Hess' law*, the equation '$\Delta H_4=0.25\times\Delta H_2+0.75\times\Delta H_3$' is suitable for Zhu's, Wang's and Kawai's data, while equation '$\Delta H_4=0.208\times\Delta H_2+0.792\times\Delta H_3$' can be applied to present authors' and HSC Chemistry's. However, Zhu's, Wang's and Kawai's data are not consistent because they neither obey the former nor the later equation. It can be seen HSC Chemistry's results completely accord with the present work and Zhu's data agree well with the authors'. Nevertheless, Kawai's are more or less deviated from the authors', HSC's and Zhu's, while Wang's data have obviously deviations from the others'.

5 Conclusions and Perspectives

(1) Three-curve-intersection principle and three-line-parallel principle and their logical justification are proposed to examine the accuracy of thermodynamic data of iron oxides reduction reactions.

(2) Sixteen empirical formulas and eight enthalpy values for iron oxide reduction reactions are obtained, which can well represent the standard data and satisfy the thermodynamic constraints. They are greatly different from those in the conventional textbooks and journals.

(3) The eutectoid temperature of the three phases of Fe_xO, Fe and Fe_3O_4, is 576℃.

As being widely told, the stoichiometric FeO is instable in the process of iron oxides reduction. So the iron oxides reduction mechanism is commonly described as, $Fe_2O_3\rightarrow Fe_3O_4\rightarrow Fe$ below 576℃ and $Fe_2O_3\rightarrow Fe_3O_4\rightarrow Fe_xO\rightarrow Fe$ above 576℃. Nevertheless, more thermodynamic and kinetic researches [16, 36-41] implemented recently have shown that the iron oxides reduction mechanism is not as so simple. Fe(II) has been observed during the reduction process below 576℃ [37, 39-41], and this cannot be interpreted by the traditional Baur-Glaessner diagram. Hence

more fundamental study focused on mechanisms of iron oxides reduction by CO and H_2 should be carried out, particularly when the sample is annealed and with impurities.

Acknowledgement

This work is financially supported by the Science & Technology Support Project of China (grant No.2011BAE04B02) and the National Natural Science Foundation of China (grant No. 51174053). Acknowledgement is also to Mrs. Liu A H for her assistance in the experimental work.

References

1. Bogdandy, L. V.; Engell, H. J. *The Reduction of Iron Ores*; Springer Verlag: Berlin, **1971**.
2. Liang, L. K.; Che, Y. C.; Yang, H.; Li, X. W. *Metallurgical Thermodynamics and Kinetics*; Northeastern University of Technology Press: Shenyang, **1990**; pp 86-90.
3. Kirkaldy, J. S.; Ward, R. G. *Aspects of Modern Ferrous Metallurgy*; University of Toronto Press: Toronto, **1964**; pp 102-105.
4. Rao Y. K. *Stoichiometry and Thermodynamics of Metallurgical Processes*; Cambridge University Press: London, **1985**; pp 726-773.
5. Han, Q. Y. *Metallurgical Kinetics*; Metallurgical Industry Press: Beijing, **1983**; pp 156-157.
6. John, F. E. *The Physical Chemistry of Steelmaking*; The Technology Press of MIT, John Wiley & Sons, Inc. & Chapman & Hall, **1956**; pp 159-164.
7. Coudurier, L.; Hopkins, D. W.; Wilkomirsky, I. *Fundamentals of Metallurgical Processes*, 2nd ed.; Pergamon Press: New York, **1985**; pp 159-162.
8. Chu, M.; Nogami, H.; Yagi, J. I. *ISIJ Int.* **2004,** 44(3), 510.
9. Chu, M.; Yagi, J. I. *Steel Res. Int.* **2010,** 81(12), 1043.
10. Bahgat, M.; Halim, K. S. A.; El-Kelesh, H. A.; Nasr M. I. *Steel Res. Int.* **2012,** 83(7), 686.
11. Barin, I. *Thermochemical Data of Pure Substances*, 3rd ed.; Wiley-Vch Verlag: Weinheim, **1995**.
12. NIST-JANAF. *Thermochemical Tables*, 4th ed.; *Journal of Physical and Chemical Reference Data Monograph*, No.9, **1998**.
13. Barin, I.; Knacke, O. *Thermochemical Properties of Inorganic Substances*, Springer-Verlag: Berlin, 1973; Supplement, **1977**.
14. Braithwaite. *Chem. News* **1895,** 72, 211.
15. Baur, L. E.; Glaessner, A. *Z. Phys. Chemie* **1903,** 354(43), 68.
16. Zhang, W.; Zou, Z. S.; Zhang, J. H.; LI, Q.; Qi, Y. H. *J. Phys. Chem. C* **2013,** submitted.
17. Schenck; Semiller and Falcke. *Chem. Ber.* **1907,** 40, 1704.
18. Schenck and Heller. *Chem. Ber.* **1905,** 38, 2132.
19. Eastman, E. D. *J. Am. Chem. Soc.* **1922,** 44(5), 975.
20. Eastman, E. D.; Evans, R. M. *J. Am. Chem. Soc.* **1924,** 46(4), 888.

21. Emmett, P. H.; Shultz, J. F. *J. Am. Chem. Soc.* **1930,** 52, 4268.
22. Emmett, P. H.; Shultz, J. F. *J. Am. Chem. Soc.* **1933,** 55, 1376.
23. Chipman, J.; Marshall, S. *J. Am. Chem. Soc.* **1940,** 62, 299.
24. Darken, L. S.; Gurry, R. W. *J Am. Chem. Soc.* **1945,** 67, 1398.
25. Darken, L. S.; Gurry, R. W. *J Am. Chem. Soc.* **1946,** 68, 789.
26. Wang, X. L. *Ferrous Metallurgy (Ironmaking Department)*; Metallurgical Industry Press: Beijing, **2002**; pp.82-85.
27. Li, H. G. *Metallurgical Theory*; Science Press: Beijing, **2005**; pp.156-206.
28. Zhu, M. Y. *Modern Metallurgy (Ferrous Metallurgy)*; Metallurgical Industry Press: Beijing, **2005**; pp.60-62.
29. Hara, Y.; Tsuchiya, M.; Kondo, S. I. *Tetsu to Hagane* **1974,** No. 9, 1261.
30. Murayama, T.; Ono, Y.; Kawai, Y. *Tetsu to Hagane* **1977,** No. 7, 1099.
31. Ono-Nakazato, H.; Yonezawa, T.; Usui, T. *ISIJ Int.* **2003,** 43(10), 1502.
32. Takahashi, R.; Takahashi, Y.; Yagi, J. I.; Omori, I. *Trans. ISIJ* **1986,** 26, 765.
33. Pineau, A.; Kanari, N.; Gaballah, I. *Thermochim. Acta* **2007,** 456, 75.
34. Conejo, A. N.; Martins, G. P. *ISIJ Int.* **1997,** 37(10), 967.
35. Hayashi, S.; Iguchi, Y. *ISIJ Int.* **1998,** 38(10), 1053.
36. El-Geassy, A. A.; Nasr, M. I. *ISIJ Int.* **1990,** 30(6), 417.
37. Pineau, A.; Kanari, N.; Gaballah, I. *Thermochim. Acta* **2006,** 447, 89.
38. Wimmers, O. J.; Arnoldy, P.; Moulijn, J. A. *J. Phys. Chem.* **1986,** 90, 1331.
39. Khader, M. M.; El-Anadouli, B. E.; El-Nagar, E.; Ateya, B. G. *J. Solid State Chem.* **1991,** 93, 283.
40. Jozwiak, W. K.; Kaczmarek, E.; Maniecki, T. P. *Appl. Catal., A-Gen.* **2007,** 326, 17.
41. Zhao, P.; Guo, P. M.; Zhang, D. W. *Iron and Steel* **2006,** 41, 12.